JOURNAL OF SOLID STATE CHEMISTRY 114, 123–128 (1995)

Stereochemical Activity of Thallium (I) Lone Pair in the Tridymite-Related Compounds $TlBePO_4$ and $TlBeAsO_4$

G. Wallez,[1] S. Jaulmes, A. Elfakir, and M. Quarton

Laboratoire de Cristallochimie du Solide, CNRS-URA 1388, Université Pierre et Marie Curie, 4, place Jussieu, 75252 Paris Cedex 05, France

Received January 20, 1994; accepted March 9, 1994

Single crystals of monophosphate $TlBePO_4$, grown by the hydrothermal process, belong to the orthorhombic space group $Pna2_1$. Unit cell contains four formulae ($Z = 4$) and crystal parameters are found to be $a = 9.286(3)$ Å, $b = 8.090(3)$ Å, $c = 4.837(1)$ Å. Rows of vertices-connected PO_4 and BeO_4 tetrahedra are laid out in planes, forming six-membered rings in which bulky thallium atoms find their place. Although clearly related to the stuffed tridymite structural type, the oxygen framework shows an unusual distortion, as in the case of monoarsenate $TlBeAsO_4$. Stereochemical activity of the partly hybridized thallium (I) $6s^2$ pair, located after calculation of the local electrostatic field, appears as the cause of this peculiarity. © 1995 Academic Press, Inc.

PREPARATION AND MORPHOLOGY OF CRYSTALS

Pure $TlBePO_4$ microcrystalline powder, obtained by solid state reaction (1), was used as a nutrient for hydrothermal growth. 3.3 g of thallium fluoride are mixed with 2.0 g of title compound and poured into a 8 cm^3 copper tube. Water is then added in suitable volume to give a 70% filling ratio before sealing up the tube. The choice of TlF as mineralizer comes out from chemical criteria: it yields a fluoride-rich solution, allowing to raise the saturation point of the nutrient without any chance of cationic exchange. The container is set in a cone-sealed refractory steel vessel, then the free inner volume is filled up with water at the same 70% ratio in order to balance the vapour pressures at high temperature.

The vessel is placed in a vertical tubular furnace, heated up to stage temperature (550°C at half-length of the vessel, 615°C at the bottom) for 3 days, then slowly cooled ($30°C \cdot hr^{-1}$). Vapour pressure during the stage is evaluated at 2400 atm from the pressure-temperature diagram of water (2). Obtained crystals are transparent, colourless, and elongated along **c** (two-fold) axis, with size ranging up to 3.0 mm along this direction. Two kinds of morphology have been observed on a NEDINSCO two-circle optical goniometer (Fig. 1), both consistent with an orthorhombic symmetry.

STRUCTURE DETERMINATION OF $TlBePO_4$

Weissenberg and precession photographs, performed on a $TlBePO_4$ single crystal, show an orthorhombic symmetry. The systematic presence criteria for observed reflections match with both *Pnma* (centric) and $Pna2_1$ (acentric) space groups, but on the basis of a positive test of second harmonic generation (laser YAG: Nd; $\lambda = 1.06$ μm), we can conclude that $TlBePO_4$ belongs to space group $Pna2_1$, as does its arsenate counterpart (3). Collection of diffracted intensities was performed at 20°C on a Syntex–Nicolet P3F four-circle diffractometer. Main acquisition parameters are summarized in Table 1.

Collected intensities were first corrected of the Lorentz and polarization factors. Because of the high linear absorption coefficient and the anisotropic shape of the crystal, absorption corrections had to be made using an analytical method (4).

Thallium atom was first located from the three-dimensional Patterson map and its position was refined with

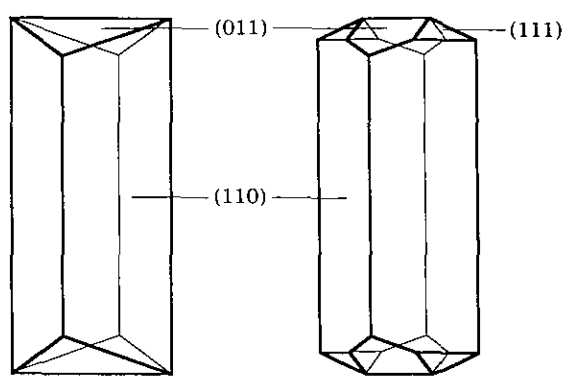

FIG. 1. Morphology of hydrothermally-grown $TlBePO_4$ crystals.

[1] To whom correspondence should be addressed.

0022-4596/95 $6.00

TABLE 1
Crystallographic and Experimental Data

Crystal data	
Formula	$TlBePO_4$
Formula weight ($g \cdot mol^{-1}$)	244.36
Crystal dimensions (mm)	0.4 × 0.08 × 0.04
a (Å)	9.286(3)
b (Å)	8.090(3)
c (Å)	4.837(1)
V (Å^3)	363.4(2)
Space group	$Pna2_1$ (33)
Z	4
$D_{calc.}$($g \cdot cm^{-3}$)	4.47
$F(000)$	528
μ (Mo$K\alpha$) (cm^{-1})	448.3
Data collection	
Scan mode	θ–2θ
Scan angle	2θ ranges from $2\theta_1$–1.0° to $2\theta_2$ + 1.0°, θ_1 and θ_2 being the diffraction angles for Mo $K\alpha_1$ and $K\alpha_2$ radiations
Recording angular range θ (°)	2–37.5
Number of independent data observed with $I > \sigma(I)$	1045 measured, 747 used in refinements
Structure solution and refinements	
Extreme values of transmission factor	0.033–0.171
Number of variables	73 (including anisotropic temperature factors for all atoms)
$R = \Sigma \lvert F_o - \lvert F_c \rvert \rvert / \Sigma F_o$	0.057
Weighting scheme	$w = 1/\sigma(F)$
$R_w = [\Sigma w \cdot (F_o - \lvert F_c \rvert)^2 / \Sigma w \cdot F_o^2]^{1/2}$	0.050
Extinction parameter refined	$g = 0.21(2) \times 10^{-6}$

an isotropic temperature factor. Electronic density maps obtained from Fourier series gave approximate coordinates of phosphorus, oxygen, and beryllium, but the electronic cloud of the thallium atom appeared unusually elongated. Instead assigning high values to its anisotropic temperature factors, we preferred to define two equally-occupied sites (referred thereafter as Tl(1) and T1(2)), 0.26 Å apart. In the next stage, refinements of atomic coordinates (Table 2) and thermal agitation parameters (Table 3) were performed by means of a modified ORXFLS program (5) using atomic diffusion factors (6).[2] Fluctuations of electronic density on the last Fourier maps are less than 1 $e \cdot Å^{-3}$. Studied sample appears as a mosaic crystal with type I secondary extinction (7); gaussian angular disorientation is $\sigma = 27''$.

TABLE 2
Fractional Atomic Coordinates and Thermal Parameters
$U_{eq} = \frac{1}{3} \Sigma_i \Sigma_j U_{ij} a_i^* a_j^* \mathbf{a}_i \cdot \mathbf{a}_j$

Atom	x	y	z	U_{eq} (10^{-3} Å^2)
Tl(1)	0.011(1)	0.334(1)	0	21(2)
T1(2)	0.031(1)	0.348(1)	0.029(2)	9(1)
Be	0.352(2)	0.614(3)	0.021(6)	8(8)
P	0.3274(4)	0.4196(5)	0.539(3)	5(2)
O(1)	0.220(1)	0.291(1)	0.440(3)	9(5)
O(2)	0.479(1)	0.344(1)	0.523(7)	29(7)
O(3)	0.301(1)	0.468(2)	0.826(3)	9(6)
O(4)	0.316(2)	0.576(2)	0.351(3)	11(6)

TABLE 3
Anisotropic Agitation Parameters (10^{-3} Å^2)

	U_{11}	U_{22}	U_{33}	U_{12}	U_{13}	U_{23}
Tl(1)	20(3)	13(2)	29(2)	0(1)	−11(3)	−10(2)
Tl(2)	14(2)	12(2)	1(1)	3(2)	6(1)	6(1)
Be	12(8)	16(9)	0(5)	4(7)	−15(10)	33(9)
P	2(2)	7(2)	7(3)	−2(1)	2(3)	−17(3)
O(1)	11(6)	4(5)	13(7)	−3(4)	−6(5)	6(4)
O(2)	14(5)	20(6)	54(10)	−2(5)	39(8)	27(9)
O(3)	10(6)	9(6)	9(6)	−8(5)	6(5)	−5(5)
O(4)	27(7)	0(3)	7(6)	5(4)	6(6)	4(5)

STRUCTURE DESCRIPTION

Depending on the size of their constituting cations, $A^IB^{II}X^VO_4$ compounds crystallize under different structural types: olivine, arcanite, glaserite, phenacite, or stuffed tridymite. Those compounds with small B^{II} and X^V (B = Be, Ni, Mg, or Zn; X = P, As, or V) and large A^I cations (A = K, Tl, Rb, or Cs) usually belong to the latter type. Thus, the oxygen framework of $TlBePO_4$ shows similarities to the well-known β-SiO_2 tridymite.

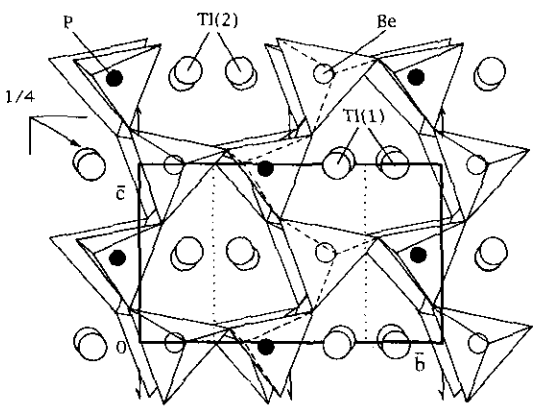

FIG. 2. Cell projection of $TlBePO_4$ along a axis.

[2] A list of values of h, k, l, F_o, and F_c can be obtained by contacting the authors.

TABLE 4
Distances (Å) and O–P–O Angles (°) in PO_4 Tetrahedron

	O(1)	O(2)	O(3)	O(4)
O(1)	1.52(2)	108(1)	111.8(9)	109(1)
O(2)	2.48(2)	1.53(2)	108(2)	111(1)
O(3)	2.47(2)	2.43(3)	1.46(2)	108.9(8)
O(4)	2.51(2)	2.55(2)	2.46(2)	1.56(2)

However, instead of hexagonal rings of SiO_4 tetrahedra following a UDUDUD order (U(up) and D (down) refer to the tetrahedron's orientation perpendicular to the rings), the skeleton is made up of twisted six-membered rings of BeO_4 and PO_4 tetrahedra adopting a UUUDDD order (Fig. 2).

Although all oxygen atoms are shared between one PO_4 and one BeO_4 tetrahedra, their roles in the oxygenated skeleton are different:

—O(1), O(2) and O(4) atoms link two tetrahedra belonging to the same layer of six-membered rings;

—O(3) atoms, pointing approximatively along **a** axis, link tetrahedra of two consecutive layers.

The PO_4 tetrahedron (Table 4) is a little flattened along the **a** axis, with O(3)–O(n) edges shorter than all others, and the phosphorus atom is slightly off-center toward O(3). Although the coordinates of the beryllium atom are known with lower accuracy because of its small atomic number, a similar shift of the central atom toward O(3) may be observed in BeO_4 (Table 5), but the tetrahedron appears rather elongated along the **a** axis.

Because of its large ionic radius ($r_i(Tl^I)$ = 1.59 Å) (8), and the twisted shape of the oxygen skeleton, the coordination polyhedron of thallium atom had to be determined by calculation of strengths of bonds shared by thallium with its nearest oxygen neighbors. The empirical method of Brown and Wu (9), based on the cation–oxygen distances, made it possible to define the same eight-anion polyhedron (made up of 2 O(1), 2 O(2), 2 O(3), and 2 O(4)) for both Tl(1) and Tl(2) sites (Table 6), the respective cumulated bond strengths (1.016 and 1.018 electrons) being in good agreement with the theoretical valence of the cation. The TlO_8 polyhedron appears as a quasi-hemispherical shape (Fig. 3) with Tl–O distances scattered over more than 0.6 Å. Therefore, each oxygen atom is bonded to one beryllium atom, one phosphorus atom, and two thallium atoms, but the sharing of valence strengths (Table 7) with the neighbor cations is slightly irregular: atom O(3), connecting tetrahedra of different (**b**, **c**) layers, is strongly tied to tetracoordinated cations, but only forms weak bonds with the neighbor thallium atoms (Tl–O distances are calculated from a Tl(0) midthallium position). O(1), O(2), and O(4) atoms belonging to hexagonal rings have opposite behavior. Similar asymmetrical interactions may be pointed out in the isostructural arsenate $TlBeAsO_4$ (3).

TABLE 5
Distances (Å) and O–Be–O Angles (°) in BeO_4 Tetrahedron

	O(1)	O(2)	O(3)	O(4)
O(1)	1.63(2)	102(2)	113(2)	108(2)
O(2)	2.52(2)	1.61(2)	117(2)	103(2)
O(3)	2.68(2)	2.72(2)	1.58(4)	112(2)
O(4)	2.66(2)	2.56(3)	2.67(2)	1.66(4)

TABLE 6
Distances (Å) around Tl Atoms

Tl(1)–Tl(2)	0.26(2)		
Tl(1)–O(4)	2.73(2)	Tl(2)–O(1)	2.69(2)
O(2)	2.74(3)	O(4)	2.76(2)
O(1)	2.90(2)	O(3)	2.86(2)
O(2)	2.93(3)	O(2)	2.89(3)
O(3)	3.02(2)	O(2)	2.94(3)
O(4)	3.20(2)	O(1)	3.38(2)
O(3)	3.24(2)	O(4)	3.39(2)
O(1)	3.35(2)	O(3)	3.47(2)

Besides their analogies with the other $ABXO_4$ compounds, $TlBePO_4$ and $TlBeAsO_4$ have specific features that previous studies, dealing only with alkaline-stuffed phases, had never reported. Cell projection along the **c** axis of $TlBePO_4$ (Fig. 4) shows an unusual distortion resulting from the tilt of BeO_4 (about 10° away from the **a** axis) and PO_4 (24°) tetrahedra. This structural anomaly may not result from the size of the inserted cation, because the ionic radius (8) of the eight-coordinated Tl^+ cation (1.59 Å) is intermediate between that of K^+ (1.51 Å) and those of Rb^+ (1.61 Å) and Cs^+ (1.74 Å). Therefore, we

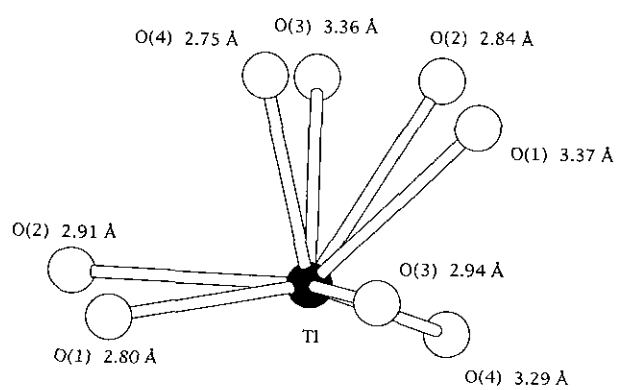

FIG. 3. Coordination polyhedron of thallium atom.

TABLE 7
Valence Units (e) Shared between O Atoms and Cations

	O(1)	O(2)	O(3)	O(4)	Sum
Tl(0)	0.24	0.31	0.19	0.27	1.01
Be	0.50	0.53	0.57	0.48	2.08
P	1.32	1.27	1.56	1.17	5.32
Sum	2.06	2.11	2.32	1.91	

had to examine the peculiarities of Tl^+: the presence of a lone electron pair and its high electronegativity.

LONE PAIR LOCALIZATION

Because of the open and irregular shape of the coordination polyhedron of the monovalent cation in stuffed tridymite structures, the location of a lone pair cannot be predicted simply from the increase of the cell volume. V/Z formula volumes of $A\text{BePO}_4$ (1, 10) and $A\text{BeAsO}_4$ (A = K, Tl, Rb, Cs) (11) plotted versus ionic radius of A^{I} (Fig. 5) show no anomalous increase for A = Tl.

Furthermore, the hybridization rate of the $6s^2$ orbital is expected to be rather low because of the high atomic number of Tl and its metallic character (12). Thus, the research on the lone pair was carried out using a self-consistent electrostatic model. Electric charges of ions were first calculated from the electronegativities of the electronic orbitals (13) on the basis of the M–O bonds orientations for oxygen, and assuming an sp^3 hybridization for tetracoordinated cations (Be, P). Hypotheses have been formulated for the Tl cation because the high energy of its inner electrons forbade similar calculation: the hybridization rate was estimated at 25%. Results for $TlBePO_4$ and $TlBeAsO_4$ are gathered in Table 8. Owing to the high electronegativity of the involved cations, Tl–O, P–O, and As–O bonds are rather covalent and calculated charges appear more realistic than formal ones.

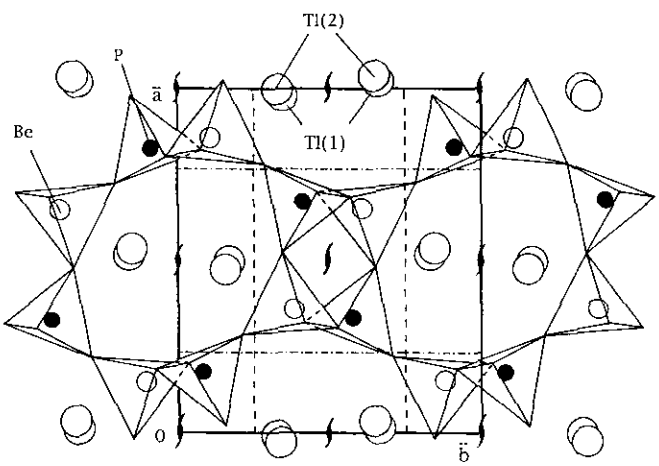

FIG. 4. Cell projection of $TlBePO_4$ along **c** axis.

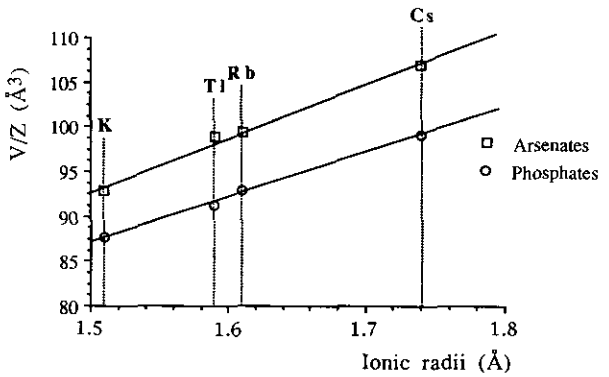

FIG. 5. Formula volumes of $A\text{BePO}_4$ and $A\text{BeAsO}_4$ vs ionic radii of A^{I}.

Electrostatic fields on Tl(1), Tl(2), and midthallium Tl(0) sites were computed from the contributions of every ion located inside a 200 × 200 × 200 Å^3 cube centered on the site. A similar process, based on the dipolar field generated from electrically neutral cells has been reported by Verbaere *et al.* (14). From the polarizability α = 5.11 Å^3 (15) of the thallium atom, the approximate shift $\boldsymbol{\delta}$ of the lone pair barycenter may be computed according to the formula $\boldsymbol{\mu} = \alpha\mathbf{E} \sim -2\boldsymbol{\delta}$. Further calculations of local field were carried out, replacing the initial q charge of the thallium cation by $(q + 2)$ and assuming a -2 charge for the lone pair, until a self-consistent position of the lone pair (thereafter referred to as E) was reached (Table 9).

The results are almost similar from one site to the other one for each compound; therefore, the Tl(0) midthallium position may be regarded as a satisfactory representation. The Tl–E dipoles show identical features in both phosphate and arsenate, according to their isomorphism. Their orientations are very close to the **c** polar axis with so small a θ angle that it may result from a lack of accuracy of initial data used in computing, so that the dipoles may actually be parallel to this axis.

TABLE 8
Electric Charges (e) of Ions

	$TlBePO_4$	$TlBeAsO_4$
Tl	+0.337	+0.349
Be	+1.663	+1.605
P/As	+0.439	+0.337
O(1)	−0.608	−0.597
O(2)	−0.632	−0.591
O(3)	−0.613	−0.569
O(4)	−0.585	−0.535

TABLE 9
Location Data of Lone Pairs in $TlBePO_4$ and $TlBeAsO_4$, where $\theta = (\vec{TlE}, c)$

	$TlBePO_4$			$TlBeAsO_4$		
	Tl(1)	Tl(2)	Tl(0)	Tl(1)	Tl(2)	Tl(0)
δ_x (Å)	0.030	−0.013	0.009	−0.022	−0.060	−0.041
δ_y (Å)	0.035	0.034	0.004	0.035	0.037	0.036
δ_z (Å)	−0.625	−0.653	−0.656	−0.680	−0.707	−0.695
δ (Å)	0.627	0.655	**0.657**	0.681	0.711	**0.697**
θ (°)	4.6	4.5	3.2	3.1	6.1	4.3

Thus, the lone pairs alternate with their carriers along rows parallel to the **c** axis, taking advantage of the **c**-directed tunnels at $x = 0$, $y = \frac{1}{2}$ and $x = \frac{1}{2}$, $y = 0$. Because the lone pair is located in the natural cavities of the structure, no additional volume needs to be expected, as was previously pointed out.

Among the eight oxygen anions surrounding thallium in $TlBePO_4$, four are close to the lone pair (2.32 to 2.84 Å), the other ones being more than 3.20 Å away. According to classical hypothesis, the mean *E*–O distance to the first ones (2.64 Å) is nearly equal to twice the ionic radius of O^{2-} (12). Assuming that the usual volume of a lone pair is almost that of an oxygen anion, the hybridization rate of the $6s^2$ pair, that is, its stereochemical activity, may be depicted by the Tl–*E*/$\overline{Tl–O}$ distance ratio ($\overline{Tl–O}$ refers to the mean thallium–oxygen distance in the coordination polyhedron). Obtained values for $TlBePO_4$ and $TlBeAsO_4$ (respectively 22 and 23%) are in good agreement with that previously used in computing the electrical charge of thallium, and attest significant stereochemical activity in both compounds.

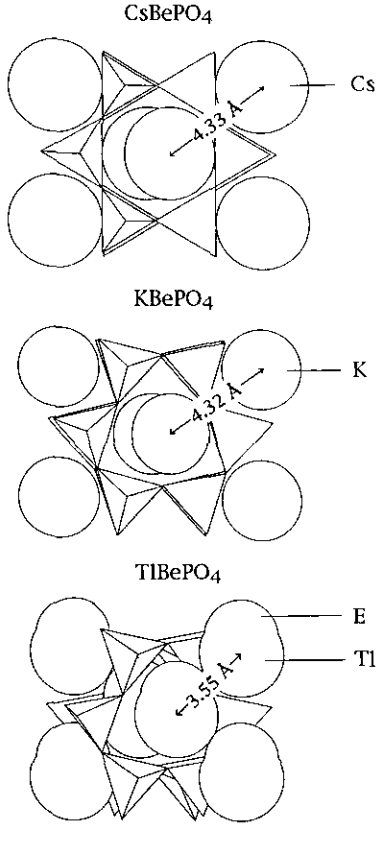

FIG. 6. Cell projections of $ABePO_4$ (A = K, Cs, Tl) with A^1 cations at real size.

DISCUSSION

Like alkaline cations in similar structures, thallium atoms are located at the intersections of the **a**-directed tunnels passing through the six-membered tetrahedra rings and the **c**-directed tunnels passing through the eight-membered rings. However, the comparison between $ABePO_4$ structures (Fig. 6) points out the singular closeness of thallium atoms, which obviously derives from the electronegativity of thallium and the presence of a lone pair:

—because of its high electronegativity (1.44) (16), the real charge of thallium and the Tl–Tl electrostatic repulsions are less than in potassium (0.91), rubidium (0.89), and cesium (0.86);

—the lone pair is attracted by the opposite side of the nearest thallium–lone pair dipole.

Thus, each lone pair comes into contact with another thallium atom, forcing its way through the usually empty spaces between two tetrahedra rows and giving an exceptionally high parameter *a*. In contrast, parameters *b* and *c* are low because of the concatenation of the thallium atoms and the monodentate skeleton, which imposes a folding of the tetrahedra layers. The cell parameters show a significant deviation from the expected pseudo-hexagonal pattern: $b/c = 0.966\ \sqrt{3}$ ($TlBePO_4$) and $0.963\ \sqrt{3}$ ($TlBeAsO_4$) instead of $0.99\ \sqrt{3}$ (mean value for A = K, Rb, or Cs).

Along with this structural distortion, the stretching of the $6s^2$ pair along the polar axis induces a permanent dielectric polarization which has been computed according to atomic coordinates and charges: $4.9\ \mu C \cdot cm^{-2}$ for $TlBePO_4$ and $5.2\ \mu C \cdot cm^{-2}$ for $TlBeAsO_4$. As expected, interesting ferroelectric properties have also been observed (17).

ACKNOWLEDGMENTS

The authors thank Mr. A. Mazurier (Laboratoire de Physique, Faculté de Pharmacie, Université Paris V) for performing the diffracted intensities collection.

REFERENCES

1. G. Wallez, A. Elfakir, and M. Quarton, *Powder Diffraction* **7**(1), 44 (1992).
2. G. C. Kennedy, *Am. J. Sci.* **248,** 540 (1950).
3. S. Jaulmes, G. Wallez, A. Elfakir, and M. Quarton, *C. R. Acad. Sci. Paris Ser. 2* **315,** 941 (1992).
4. J. de Meulenaer and H. Tompa, *Acta Crystallogr. Sect. A* **19,** 1014 (1965).
5. W. R. Busing, *Acta Crystallogr. Sect. A* **27,** 683 (1971).
6. "International Tables for X-Ray Crystallography," Vol. VI. Kynoch, Birningham, 1974.
7. P. Becker and P. Coppens, *Acta Crystallogr. Sect. A* **30,** 129 (1974).
8. R. D. Shannon, *Acta Crystallogr. Sect. A* **32,** 751 (1976).
9. I. D. Brown and K. K. Wu, *Acta Crystallogr. Sect. B* **32,** 1957 (1976).
10. R. Masse and A. Durif, *J. Solid State Chem.* **73,** 468 (1988).
11. G. Wallez, Thèse de Doctorat. Université P. et M. Curie (Paris VI), 1993.
12. J. Galey, G. Meunier, S. Anderson, and A. ÅSTRÖM, *J. Solid State Chem.* **13,** 142 (1975).
13. J. P. Jolivet and M. Henry, "Better Ceramics Through Chemistry," Proceedings of the 5th Material Research Society Meeting. San Francisco, 1992.
14. A. Verbaere, R. Marchand, and M. Tournoux, *J. Solid State Chem.* **23,** 383 (1978).
15. J. Shanker and S. C. Agarwal, *Indian J. Pure Appl. Phys.* **14**(1), 79 (1976).
16. A. L. Allred and E. G. Rochow, *J. Inorg. Nucl. Chem.* **5,** 264 (1958).
17. G. Wallez, S. Jaulmes, A. Elfakir, and M. Quarton, *J. Phys. III, France* **4,** 1197–1209 (1994).